

Influence of chemical size distribution on optical properties for ambient submicron particles during severe haze events

Wenfei Zhu^a, Jiangkun Xie^a, Zhen Cheng^{a,*}, Shengrong Lou^{b,**}, Lina Luo^a, Weiwei Hu^{c,d}, Jing Zheng^e, Naiqiang Yan^a, Bill Brooks^f

^a School of Environmental Science and Engineering, Shanghai Jiao Tong University, Shanghai, 200240, China

^b State Environmental Protection Key Laboratory of Formation of Urban Air Pollution Complex, Shanghai Academy of Environmental Sciences, Shanghai, 200233, China

^c Cooperative Institute for Research in the Environmental Sciences, University of Colorado, Boulder, CO, USA

^d Department of Chemistry and Biochemistry, University of Colorado, Boulder, CO, USA

^e State Key Joint Laboratory of Environmental Simulation and Pollution Control, College of Environmental Sciences and Engineering, Peking University, Beijing, 00871, China

^f Aerodyne Research, Inc., Billerica, MA, USA



ARTICLE INFO

Keywords:

Scattering coefficients
Chemical composition
Size distribution
PM₁
Shanghai

ABSTRACT

Despite of extensive efforts on investigation into characteristics of severe haze pollution in megacities of China, the accurate relationships among the aerosol composition, mass-size distribution and optical properties during pollution episodes remain poorly understood. Here, we conducted in situ measurements of the mass size distribution of submicron aerosol (PM₁) species by using a High-Resolution Time-of-Flight Aerosol Mass Spectrometer (HR-ToF-AMS), particle light scattering by a Cavity Attenuated Phase Shift ALBedo monitor (CAPS-ALB) and a Photoacoustic Extinctionmeter (PAX) during the winter of 2017 in Shanghai, China. The average PM₁ concentration was $85.9 \pm 14.7 \mu\text{g}/\text{m}^3$ during the haze episodes, of which was ~ 7 times higher than that of clean period ($12.1 \pm 3.1 \mu\text{g}/\text{m}^3$). Organic aerosol (OA) and inorganic species ($\text{SO}_4^{2-} + \text{NO}_3^- + \text{NH}_4^+$) contributed 39.9% and 51.2% of the total mass of PM₁ during the haze episodes, respectively. OA exhibited a single or bimodal distribution during the haze episodes with the peak concentration of $51.8 \mu\text{g}/\text{m}^3$. There were no obvious differences between ammonium nitrate (NH_4NO_3) and ammonium sulfate ($(\text{NH}_4)_2\text{SO}_4$) during the haze episodes, which exhibited single peak distributions at the sizes of 650–700 nm and ~ 700 nm, respectively. The peak positions of OA, NH_4NO_3 and $(\text{NH}_4)_2\text{SO}_4$ in clean period were in the range of 450–500 nm, 550–600 nm and 450–500 nm with the peak concentrations of $5.5 \mu\text{g}/\text{m}^3$, $3.1 \mu\text{g}/\text{m}^3$ and $3.8 \mu\text{g}/\text{m}^3$, respectively. The increased scattering coefficients in the haze episodes were positively correlated with higher secondary inorganic aerosols and organic aerosol (OA). The high scattering coefficient contribution fraction peak diameter of NH_4NO_3 and $(\text{NH}_4)_2\text{SO}_4$ were in the range of 600–800 nm and 600–750 nm with the peak scattering coefficient of 352.6 Mm^{-1} and 165.7 Mm^{-1} , respectively. The size distribution of scattering for OA showed bimodal modes during all episodes. OA and NH_4NO_3 were the largest contributors to scattering coefficients of PM₁ during the haze episodes, accounting for 45.5% and 37.8%, respectively. The contribution of $(\text{NH}_4)_2\text{SO}_4$ to the scattering (24%) exceeded that of NH_4NO_3 during clean period. Our results elucidated that substantial changes in the aerosols optical properties due to the changes in chemical compositions and size distribution during the haze events.

1. Introduction

In recent years, haze has occurred frequently during winter in the Yangtze River Delta (YRD) region of China, especially in megacities such as Shanghai (Xu and Penner, 2012). High concentrations of

particulate matter (PM), especially PM₁ (PM with aerodynamic diameter $\leq 1 \mu\text{m}$), exert significant direct impacts on visibility degradation through optical absorption and scattering effects. The aerosol absorption and scattering effect can be determined by the size distribution and the concentration of chemical composition (Seinfeld and Pandis, 2012).

* Corresponding author.

** Corresponding author.

E-mail addresses: chengz88@sjtu.edu.cn (Z. Cheng), lousr@saes.sh.cn (S. Lou).

<https://doi.org/10.1016/j.atmosenv.2018.08.003>

Received 27 February 2018; Received in revised form 31 July 2018; Accepted 4 August 2018

Available online 06 August 2018

1352-2310/© 2018 Elsevier Ltd. All rights reserved.

Table 1
Measured Indices, time resolution and Instruments used in this work.

Measurement index	Instrument (manufacturer)	Time resolution
PM ₁ chemical species (Org, SO ₄ ²⁻ , NO ₃ ⁻ , NH ₄ ⁺ , Cl ⁻) chemical species size distribution (Dry, 30 nm ~ 1 μm)	SP-AMS Soot-Particle Aerosol Mass Spectrometer (Aerodyne Research Inc., USA)	4 min
PM _{2.5} mass concentration	FH62 C-14 β-ray (Thermo Scientific Co., MA)	5 min
PM ₁ scattering coefficient (RH ≤ 40%, 525 nm)	CAPS-ALB Cavity Attenuated Phase Shift ALBedo monitor (Shoreline Science Research Inc., Japan)	1 s
Single scattering albedo (RH ≤ 40%)	PAX Photoacoustic Extinctionmeter (Droplet Measurement Technologies Inc., USA)	
PM ₁ black carbon mass concentration (BC)	PAX Photoacoustic Extinctionmeter (Droplet Measurement Technologies Inc., USA)	5 min
Ambient RH and Temperature airport	Met one station (Met One Co., OR, USA)	30 min
Wind Speed and Wind Direction airport		30 min

The extinction efficiency of particles also varies with particle size, and the maximum is distributed in the range of 400–700 nm. Moreover, the combination of various aerosol compounds and complicate mixing states increases the complexity of the interaction between aerosols and light (Hand and Malm, 2007).

There are growing needs for a better understanding of atmospheric aerosol optical properties. The Interagency Monitoring of Protected Visual Environments (IMPROVE) algorithm has been widely used to estimate aerosol extinction in the view of chemical species known for mass extinction efficiency and hygroscopicity (Pitchford et al., 2007). The relationship between optical properties and aerosol chemical composition in China has been investigated by many studies using the IMPROVE formula, e.g., in the Pearl River Delta (PRD) region (Garland et al., 2008; Tao et al., 2014) and in the northern region (Huang et al., 2010; Roger et al., 2009; Yang et al., 2012). Those studies contributed to the knowledge of the relationship between optical properties and aerosol mass concentration, but the IMPROVE algorithm used in those studies could not investigate the effect that the particle size distribution has on the optical properties. The optical properties of particle light are also closely related to the size distributions of different chemical species in aerosols. Mie theory estimates extinction coefficients by measuring the size distributions of particles or chemical species in ambient air and the associated refraction index, thus, it can be used to explore the extinction effect of particles or chemical species under different size distribution estimates (Watson et al., 2008). Cheung et al. (2005) used this method to estimate extinction coefficients of chemical species in Guangzhou (Cheung et al., 2005). In most previous studies in China, Mie theory was applied with off-line measurements results of chemical compounds at various size distribution, whose time resolution was quite low (e.g. 12/24 h). In contrast, atmospheric aerosols usually participate in a variety of physical and chemical processes in a short period, e.g., condensation, gas-particle partitioning and photochemical oxidation (Jimenez et al., 2009; Pöschl, 2005). The traditional method of aerosol sampling combined with Mie theory estimation is difficult to characterize the evolution of haze episodes.

To track the highly time-resolved evolution of aerosol optical and chemical properties during haze events, simultaneous measurements of optical properties, chemical mass and mass-size distribution with high time resolution instrument are needed. The High-Resolution Time-of-Flight Aerosol Mass Spectrometer (HR-ToF-AMS) has made a significant contribution to study the mass-size distribution of chemical compositions (Hu et al., 2013; Li et al., 2015). Huang et al. (2013) combined an HR-ToF-AMS with a single particle soot photometer (SP2) to investigate aerosol chemical pollution characteristics in the YRD. Through high-resolution mass spectrometer, He et al. (2011) reported that the concentration of chemical compositions and the source of organic aerosol varied in high time resolution, which provided insight into the causes of fine particle pollution. However, few studies have been reported on the highly time-resolved variations in the relationship between the optical properties of aerosol and the mass-size distributions of chemical components during haze periods in China up to now.

In this study, we deployed multiple high time-resolution instruments to analyze the evolution of urban aerosol properties in Shanghai,

the megacity of China, in terms of the variance between pollution and clean periods in winter. We used HR-ToF-AMS to measure the mass concentration and size distribution of chemical compositions in non-refractory submicron particles (PM_{1^{nr}}). The aerosol optical parameters (e.g., scattering coefficients, and single scattering albedo) were monitored by a Cavity Attenuated Phase Shift ALBedo monitor (CAPS-ALB) and a Photoacoustic Extinctionmeter (PAX). The purposes of this study are 1) to understand the mass-size distribution of chemical compositions of PM₁ in haze episodes and clean periods; 2) to evaluate the practicability of Mie theory in scattering calculation via comparing the results with the measured scattering in the urban environment; 3) to investigate the influence of chemical composition and size distribution of ambient aerosols on their optical properties.

2. Experimental methods

2.1. Field campaign

The observation station (31.10°N, 121.25°E) was situated at Shanghai Academy of Environmental Sciences, located in Xuhui district of Shanghai. No obvious industrial sources were nearby. All instruments utilized in this study were placed in an air-conditioned room at the top of a nine-floor building, approximately 32 m above the ground. The observation campaign was from November 28, 2016 to January 12, 2017. Table 1 summarizes the basic instrumental information about the instruments used to measure aerosol mass concentration, chemical species, size distributions, scattering coefficient and meteorological parameters. The mass concentration and size distribution of PM_{1^{nr}} species, including OA, nitrate, sulfate, ammonium and chloride, were measured by an HR-ToF-AMS with 4 min time-resolution. The ambient air was sampled into the HR-ToF-AMS through the center of the copper at a flow rate of ~0.1 L/min. A PM URG cyclone (URG-2000-30ED) and a Naffion dryer were employed for removing coarse particles and drying aerosol particles, respectively. A PAX instrument was applied to measure the aerosol scattering coefficient, extinction coefficient ($\lambda = 532$ nm) of aerosol particles, single scattering albedo and the mass concentration of black carbon (BC). The light scattering coefficient and extinction coefficient were measured in situ using the CAPS-ALB ($\lambda = 530$ nm) with 1 s resolution. To acquire particle size of PM₁ and eliminate the effects of humidity, a PM₁ cyclone and a diffusion dryer were installed in front of the PAX and CAPS-ALB to keep relative humidity (RH) less than 40%. PM_{2.5} mass concentrations were measured by a β-ray apparatus with a time resolution of 5 min. The meteorological variables were derived from a Met one station.

2.2. Data analysis

Details of the AMS have been presented in previously published works (Canagaratna et al., 2015; Ng et al., 2010). Here, we only give a brief description of the instrument and its operation. The mass concentration and size distribution of PM_{1^{nr}} species were analyzed using the ToF-AMS standard data analysis software (SQUIRREL version 1.57 and PIKA version 1.16). The collection efficiency (CE) of 0.5 was used

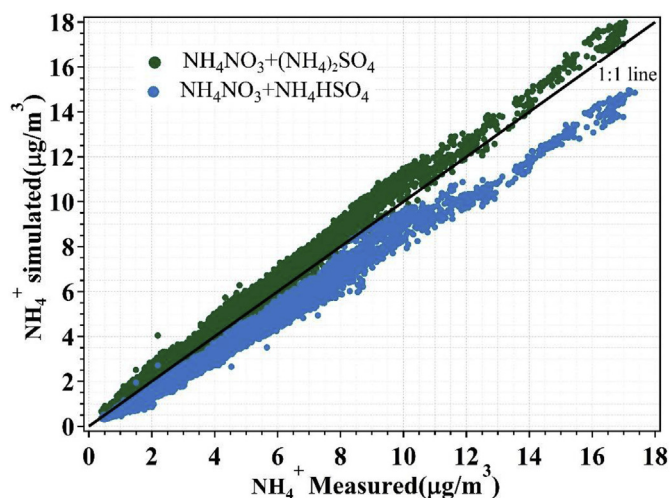


Fig. 1. Relationship between simulated NH_4^+ and measured NH_4^+ during the sampling period. The green dots are in the form of NH_4NO_3 and $(\text{NH}_4)_2\text{SO}_4$ in the atmosphere. The blue dots are in the form of NH_4NO_3 and NH_4HSO_4 in the atmosphere. The black line is the 1:1 line between simulated NH_4^+ and measured NH_4^+ . (For interpretation of the references to color in this figure legend, the reader is referred to the Web version of this article.)

for mass concentrations quantification (Matthew et al., 2008). The relative ionization efficiency (RIE) values applied in this study were 1.1 for nitrate, 1.2–1.28 for sulfate, 4.0–4.2 for ammonium, 1.3 for chloride and 1.4 for OA (Jimenez et al., 2003).

The presence of ammonium was predicted by comparing the calculated ammonium concentration with measured ammonium concentration in two formation status, i.e., $\text{NH}_4\text{NO}_3 + \text{NH}_4\text{HSO}_4$ and $\text{NH}_4\text{NO}_3 + (\text{NH}_4)_2\text{SO}_4$. Fig. 1 shows the relationship between simulated NH_4^+ and measured NH_4^+ during the sampling period. It was found that the points that exist in the form of $\text{NH}_4\text{NO}_3 + (\text{NH}_4)_2\text{SO}_4$ were almost on the 1:1 line, indicating SO_4^{2-} and NO_3^- particles mainly in the form of ammonium salts in our site. The mass concentrations of $(\text{NH}_4)_2\text{SO}_4$ and NH_4NO_3 were calculated by multiplying the AMS reported sulfate and nitrate concentration by factors of 1.37 and 1.29, respectively. The values of 1.37 and 1.29 were the relative molecular mass ratios of ammonium sulfate to sulfate and ammonium nitrate to nitrate, respectively.

Mie theory can be used to calculate the scattering efficiency (Q_{sca}) for single spherical particle of aerosol species (*index j*) by inputting the refractive index (n_j), particle diameter (D_p) and incident wavelength (λ) (Bohren and Huffman, 2008; Matzler, 2002). The PM_{10} aerosol species scattering coefficient ($\text{bsca}(j, \text{PM}_{10})$) was estimated using Eq. (1), given the particle density (ρ_j) and mass-size distribution ($C_{j, D_{\text{bin}}}$). D_{bin} was the median geometric particle size. The refractive index and density of NH_4NO_3 , $(\text{NH}_4)_2\text{SO}_4$, and OA were obtained from study (Pitchford et al., 2007) with a selected wavelength of 550 nm, as shown in Table 2.

Table 2

The Complex Relative Refractive Index and Density of various Aerosol Compositions at Dry Condition.

Chemical composition	Density	Complex relative refractive index	Reference
Organic matter	1.4	1.55 + 0.0i	(Pitchford et al., 2007)
NH_4NO_3	1.73	1.57 + 0.0i	(Pitchford et al., 2007)
$(\text{NH}_4)_2\text{SO}_4$	1.77	1.52 + 0.0i	(Pitchford et al., 2007)

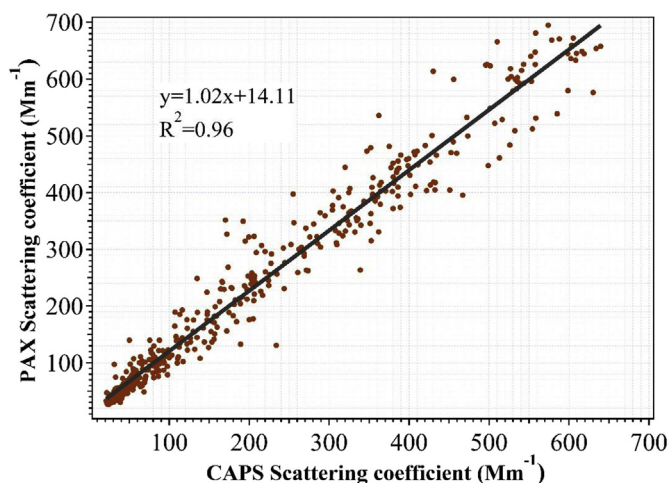


Fig. 2. Linear correlations between CAPS and PAX scattering coefficient. The time resolutions of the data sets are 1 h.

$$\text{bsca}(j, \text{PM}_{10}) = \sum_{D_{\text{bin}} < 1 \mu\text{m}} \frac{3}{2\rho_j D_{\text{bin}}} Q_{\text{sca}}(n_j, D_{\text{bin}}, \lambda) \times C_{j, D_{\text{bin}}} \quad (1)$$

2.3. Quality assurance and quality control (QA/QC)

QA/QC primarily included the routine maintenance and calibration of instruments. According to the standard procedure, the inlet flow, ionization efficiency (IE), and particle size for AMS were calibrated at the beginning and middle as well as the end of the campaign (Drewnick et al., 2005). The AMS was calibrated for IE and particle size by using size-selected pure ammonium nitrate particles. CAPS and PAX were regularly calibrated for the scattering coefficient with mono-disperse polystyrene latex spheres.

PM_{10} (= $\text{PM}_{10}^{\text{nr}} + \text{BC}$) mass measured by AMS and PAX showed good agreements with $\text{PM}_{2.5}$ measured by the β -ray instrument (Fig. 3). The detection limits of chemical species for AMS were calculated as its three times of the minimum uncertainty in the filtered air (Zhang et al., 2005). The detection limits of nitrate, sulfate, ammonium, chloride, and OA in this study were estimated to be 0.01, 0.015, 0.06, 0.03, and 0.06 $\mu\text{g}/\text{m}^3$, respectively.

The PM_{10} scattering coefficient measured by PAX showed good correlation with that from CAPS ($R^2 = 0.96$, slope = 1.02) (Fig. 2), indicating the reliability of the scattering coefficient measurements during this study.

3. Results and discussion

3.1. Evolution of severe haze episodes

The PM_{10} mass concentrations varied greatly throughout the study ranging from 3.5 to 145.0 $\mu\text{g}/\text{m}^3$, with an average of $33.0 \pm 23.8 \mu\text{g}/\text{m}^3$ over the sampling period (Fig. 3). The average mass concentrations of OA and secondary inorganic species (SIA, $\text{SIA} = \text{SO}_4^{2-} + \text{NO}_3^- + \text{NH}_4^+$) are shown in Table 3. OA and SIA varied from 1.1 to 135.1 $\mu\text{g}/\text{m}^3$ and from 1.5 to 76.1 $\mu\text{g}/\text{m}^3$, with an average of $13.0 \pm 10.5 \mu\text{g}/\text{m}^3$ and $16.3 \pm 13.1 \mu\text{g}/\text{m}^3$, respectively. The predominant inorganic species are SO_4^{2-} , NO_3^- and NH_4^+ , which altogether contributed nearly 50% of the PM_{10} mass. OA was the predominant contributor, accounting for 39.3% of PM_{10} mass. As shown in Table 3, the average dry light scattering coefficient was $174 \pm 143 \text{ Mm}^{-1}$. The single scattering albedo was 0.87 ± 0.06 (the ratio of scattering coefficient to extinction), which suggests the light extinction coefficient in Shanghai is determined by scattering coefficient. Similar values for a single scattering albedo have also been found

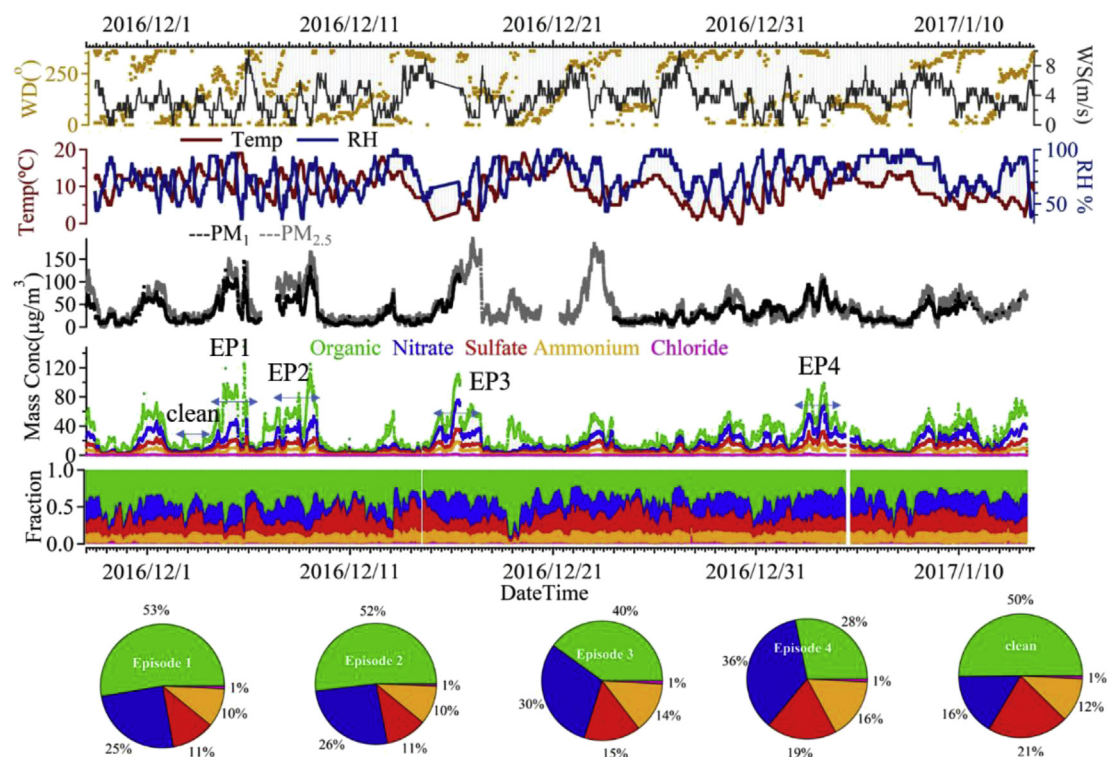


Fig. 3. Time series of meteorological variables (RH, T, WS & WD), PM₁ species (Org, SO₄²⁻, NO₃⁻, NH₄⁺, Cl⁻), PM₁ (AMS + BC), and PM_{2.5} for the entire study.

in Beijing, China (Yu et al., 2011), Kanpur and India (Ram et al., 2012).

Fall and winter are generally considered to be the most polluted seasons in China (Huang et al., 2013). Three or four episodes during January in previous years have been reported in Beijing (Sun et al., 2014). In this study, Episode is defined as the period when the scattering coefficient exceeds the sum of the average value and two standard deviations also lasting several consecutive hours. Accordingly, there were four episodes occurring during the field campaign, as summarized in Table 3, including Episode 1 (12/04 22:00–12/5 10:00, 2016), Episode 2 (12/8 19:00–12/09 08:00, 2016), Episode 3 (12/16 02:00–12/17 10:00, 2016) and Episode 4 (01/03 03:00–01/03 09:00, 2017). Similarly, a clean period (12/02 00:00–12/02 18:00, 2016) with low level of scattering coefficient was selected for comparison.

The average scattering coefficients of the selected four haze events were $529.3 \pm 47.1 \text{ Mm}^{-1}$ for Episode 1, $523.1 \pm 55.9 \text{ Mm}^{-1}$ for

Episode 2 and $486.6 \pm 61.9 \text{ Mm}^{-1}$ for Episode 4. The PM₁ mass concentrations for Episodes 1, 2, 3 and 4 were $94.0 \pm 5.8 \mu\text{g}/\text{m}^3$, $91.7 \pm 17.5 \mu\text{g}/\text{m}^3$, $70.9 \pm 21.9 \mu\text{g}/\text{m}^3$ and $87.1 \pm 13.1 \mu\text{g}/\text{m}^3$, respectively (Table 3). The average scattering coefficient for Episode 3 was not calculated, due to a lack of large amount of data concerning the measured scattering coefficient in Episode 3. Compared with the PM₁ scattering coefficient in Beijing, China, the PM₁ scattering coefficient in haze events considered in our study was much higher than that observed during the winter heating period in 2012 (323.0 Mm^{-1}) (Wang et al., 2015). As shown in Table 3, wind speeds (2.6 m/s) and temperature ($11.2 \text{ }^\circ\text{C}$) during clean period indicated greater vertical mixing and horizontal dispersion than those observed during the pollution period (Episodes 1, 2, 3 and 4), resulting in a lower PM₁ mass concentration during clean period. The average PM₁ concentrations during haze episode was $85.9 \mu\text{g}/\text{m}^3$, which was 7 times higher than that

Table 3

A Summary of Average Meteorological Parameters, PM₁ Species and Gaseous Species, and Light Scattering Coefficient During the four sub-periods, clean period and The Whole Sampling.

	Episode 1 (2016.12.04 22:00–2016.12.05 10:00)	Episode 2 (2016.12.08 19:00–2016.12.09 08:00)	Episode 3 (2016.12.16 02:00–2016.12.17 10:00)	Episode 4 (2017.01.03 03:00–2017.01.03 09:00)	Clean period (2016.12.02 0:00–2016.12.2 18:00)	Whole Sampling (2016.11.28–2017.01.13)
Meteorological parameters						
WS (m/s)	1.0 ± 0.7	2.0 ± 1.2	2.6 ± 1.5	1.9 ± 0.8	2.6 ± 1.1	3.6 ± 1.9
T ($^\circ\text{C}$)	10.5 ± 2.3	9.1 ± 1.4	4.6 ± 2.3	7.8 ± 1.1	11.2 ± 2.8	10.0 ± 3.7
RH (%)	91.8 ± 6.9	78.4 ± 12.1	68.6 ± 14.3	91.7 ± 2.6	62.3 ± 12.0	74.8 ± 15.0
PM₁ species ($\mu\text{g}/\text{m}^3$)						
Org	44.6 ± 8.5	44.2 ± 15.1	24.7 ± 7.7	23.8 ± 4.3	5.3 ± 1.5	12.9 ± 10.5
SO ₄ ²⁻	9.6 ± 1.1	8.7 ± 2.0	9.5 ± 3.9	15.3 ± 1.4	2.2 ± 0.5	5.2 ± 3.2
NO ₃ ⁻	21.4 ± 3.7	21.9 ± 5.6	20.0 ± 9.1	30.1 ± 4.2	1.8 ± 0.7	7.3 ± 6.9
NH ₄ ⁺	8.7 ± 1.3	8.6 ± 2.1	8.8 ± 3.9	13.7 ± 1.6	1.2 ± 0.3	3.8 ± 2.9
Cl ⁻	0.6 ± 0.1	0.5 ± 0.2	0.6 ± 0.4	0.7 ± 0.1	0.09 ± 0.03	0.3 ± 0.3
BC	9.2 ± 1.0	7.8 ± 1.2	7.1 ± 2.8	4.7 ± 0.6	1.4 ± 0.5	2.7 ± 2.1
PM ₁	94.0 ± 5.8	91.7 ± 17.5	70.9 ± 21.9	87.1 ± 13.1	12.1 ± 3.1	33.0 ± 23.8
Scattering coefficient						
bsca (M/m)	529.3 ± 47.1	523.1 ± 55.9	/	486.6 ± 61.9	76.1 ± 30.8	174.4 ± 144.0

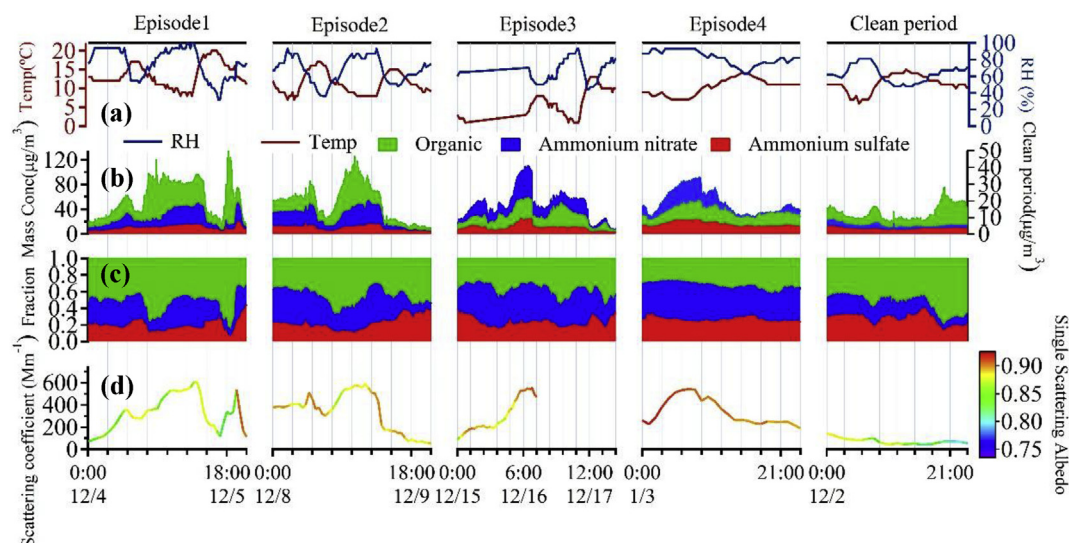


Fig. 4. Time series of chemical species characterization under dry conditions during the four haze pollution Episodes and one clean episode. (a) meteorological variables (RH; temperature); (b) mass concentration; (c) mass fraction of total mass; (d) the scattering coefficient and single scattering albedo.

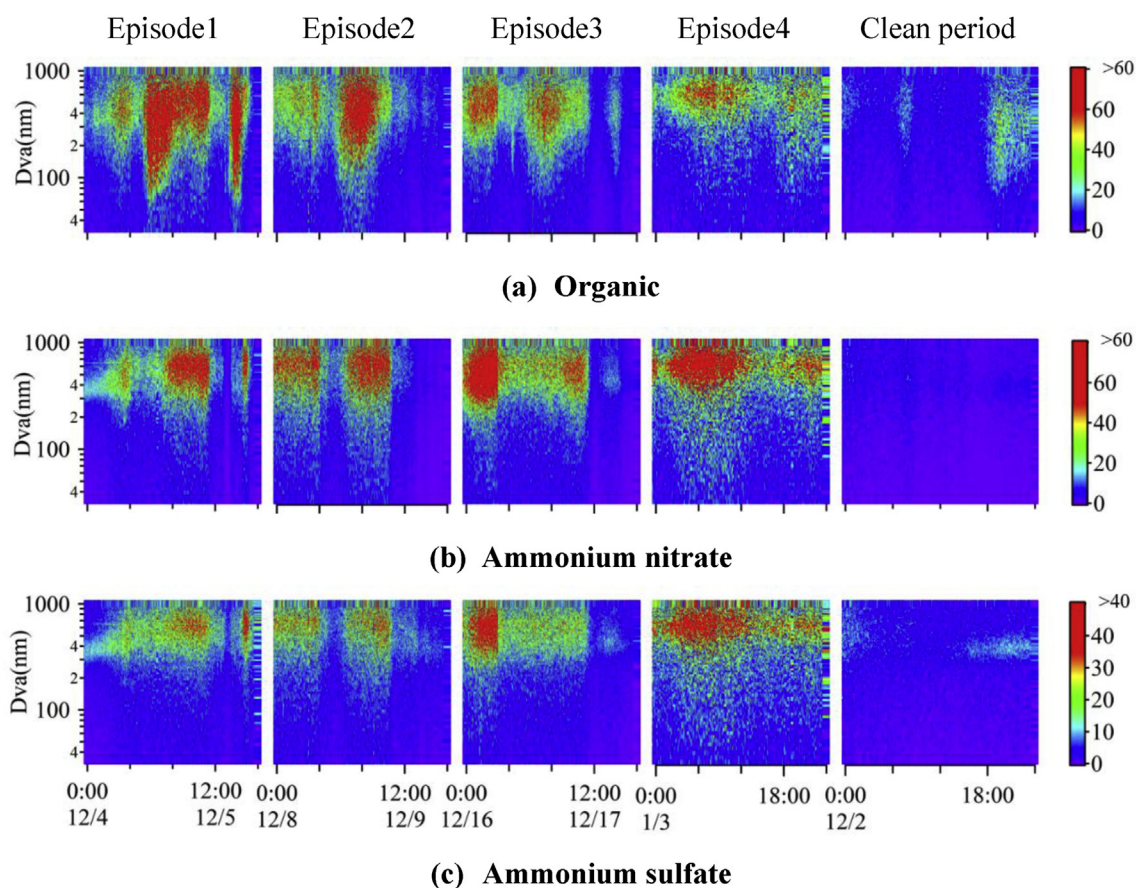


Fig. 5. Time series of size-segregated mass concentration of chemical compounds (Organic(a), Ammonium nitrate(b) and Ammonium sulfate(c)) during the four sub-periods and clean period. The plots are color coded by $dM/d\log_{10}d_{va}$ (unit: $\mu\text{g}/\text{m}^3$) of organic, ammonium nitrate and ammonium sulfate, respectively. The values exceed the range of color scale are colored with the last color (red in the figure). (For interpretation of the references to color in this figure legend, the reader is referred to the Web version of this article.)

observed during clean period. The increased scattering coefficient during episodes was associated with higher concentrations of secondary inorganic aerosols ($\text{SIA} = \text{SO}_4^{2-} + \text{NO}_3^- + \text{NH}_4^+$) and OA, when RH was in the range of 75–95% (Fig. 4), which was consistent with that reported in Beijing (Sun et al., 2014). The average mass concentrations of OA and SIA during Episodes were $34.3 \mu\text{g}/\text{m}^3$ and $44.0 \mu\text{g}/\text{m}^3$,

respectively, and were 6–9 times higher than those of the clean period.

The above four haze episodes showed various scattering coefficients and dominant chemical components (shown in Fig. 4). In Episodes 1 and 2, the OA increased dramatically as the wind speed decreased. The OA accounted for more than 50% of the mass fraction in both Episodes 1 and 2. The proportions of chemical compositions as a function of PM_{10}

are shown in Fig.S1. With the increase in PM_{10} , the proportions of OA in PM_{10} increased gradually, indicating that the enhancement of OA primarily contributed to the increase in PM_{10} during Episodes 1 and 2. The concentration percentage of OA increased from ~40% to ~70% as the events evolved, with absolute value increasing from ~20 to ~71 $\mu\text{g}/\text{m}^3$ in Episodes 1 and 2.

Secondary inorganic aerosols (SIA) were the predominant component during Episodes 3 and 4 (Fig. 4). The OA fraction decreased and the proportions of NH_4NO_3 generally exceeded that of OA in Episodes 3 and 4 (Fig.S1 and Fig. 4). From the beginning of Episode 3, the concentration of NH_4NO_3 and $(\text{NH}_4)_2\text{SO}_4$ increased rapidly on the morning of December 16 (Fig. 4). The mass concentrations of NH_4NO_3 and $(\text{NH}_4)_2\text{SO}_4$ jumped to approximately two times of those in Episodes 1 and 2, which was consistent with the increase in RH and decrease in temperature (Hu et al., 2016; Zhang et al., 2017). Correspondingly, the scattering coefficient grew rapidly from 200 to 600 Mm^{-1} (Fig. 4). Tiny differences were also identified in the mass contributions between Episodes 3 and 4, which were secondary inorganic aerosol-dominated events. Compared to Episode 3, NH_4NO_3 reached as high as 45.7 $\mu\text{g}/\text{m}^3$ and was nearly constant throughout Episode 4, but it had a lower rate of increase than $(\text{NH}_4)_2\text{SO}_4$ did. Accordingly, the mass percentage of ammonium sulfate increased continuously from ~10% at the beginning to ~20% until the peak pollution hour, and it then decreased quickly with the pollution dissipation. Ammonium sulfate accounted for approximately 38% throughout Episode 4. The proportions of SIA, especially nitrate increased and have larger contribution under high RH during Episodes 3 and 4 (Fig.S1 and Fig. 4). The results imply that SIA formation in Episodes 3 and 4 could be substantially attributed to the aqueous-phase reactions under high RH, consistent with previous studies in Beijing (Hu et al., 2017; Sun et al., 2013).

3.2. Mass size distribution of PM_{10} species

The dynamic variations of the size-segregated mass concentration of the major chemical compounds are summarized in Fig. 5. For OA in Episode 1, a high value mass loading value occurred from 18:00, 4 December to 10:00, 5 December. The whole range for size distributions of OA greatly increased at 18:00 on 4 December. Approximately 80% of the OA were distributed in the large sizes (> 400 nm). In contrast, for NH_4NO_3 and $(\text{NH}_4)_2\text{SO}_4$, the mass loading of sizes lower than 250 nm were nearly constant and fairly low (2.5 $\mu\text{g}/\text{m}^3$ for ammonium nitrate and 0.8 $\mu\text{g}/\text{m}^3$ for ammonium sulfate) from about 19:00 on 4 December to 10:00 on 5 December in Episode 1. The mass loading of sizes larger than 500 nm increased 1–2.5 times than those observed in clean period. The peak size positions for NH_4NO_3 and $(\text{NH}_4)_2\text{SO}_4$ were distributed in the ranges of 600–700 nm and 650–750 nm, respectively. Takegawa et al. (2009) observed similar particle growth of vacuum aerodynamic diameter (D_{va}) from ~100 nm to 500 nm due to the formation of secondary species during periods of stagnant conditions during summer in Beijing (Takegawa et al., 2009).

In Episode 2, the pollution status was severe with PM_{10} levels of 91.7 $\mu\text{g}/\text{m}^3$. The $PM_{2.5}$ mass concentration at the same time reached approximately 150 $\mu\text{g}/\text{m}^3$ (Fig. 3). The high ratio of PM_{10} to $PM_{2.5}$ indicates that the small size particles account for a significant fraction of mass concentration. The OA mass concentration remained at a high level from 22:00 on 8 December to 3:00 on 9 December. The transition to slightly smaller sizes (300 nm) was seen over time in the average mass size distributions. The size distribution of OA mass concentration ranked in the order of 300–600 nm > 650–750 nm > 200–300 nm > 750–1000 nm > 0–200 nm. The size distribution of NH_4NO_3 in Episode 2 was similar to that of Episode 1, however, about 78% of the NH_4NO_3 mass concentration was contributed by particles with diameters larger than 450 nm, compared with 35% of that in Episode 1. Thus, a similar OA-dominated pollution event occurred in Episodes 1 and 2, in which the average mass concentration of $(\text{NH}_4)_2\text{SO}_4$ remained at a constant value, but the NH_4NO_3 increased in

the large size range. From Episode 1 to 2, NH_4NO_3 in large size range elevated, whereas the small size particle (< 300 nm) of $(\text{NH}_4)_2\text{SO}_4$ was present at concentrations as low as 1.0 $\mu\text{g}/\text{m}^3$. Unlike NH_4NO_3 , the size distribution of $(\text{NH}_4)_2\text{SO}_4$ in Episode 2 could be divided into two different patterns. In the first 8 h in Episode 2, the size distribution of $(\text{NH}_4)_2\text{SO}_4$ was stable at 7.7 $\mu\text{g}/\text{m}^3$ and particles in the large size range (> 500 nm) were presented in the same way that NH_4NO_3 was observed previously. After about 4:00 on 9 December, the particle mass with sizes from 350 nm to 500 nm increased rapidly from 7.3 $\mu\text{g}/\text{m}^3$ to 14.5 $\mu\text{g}/\text{m}^3$, which was twice as high as that of $(\text{NH}_4)_2\text{SO}_4$ in the first stage. Kong et al. (2014) found that sulfate and nitrate have a negative correlation in urban sites in Shanghai. They also confirmed that chemical processes and meteorological conditions might have different effect on the formation of these two secondary inorganic species (Kong et al., 2014). At the end of Episode 2 about 9:00 on 9 December, the wind blew from the northeast with a faster speed than pollution stage contributed to the decrease of PM_{10} species concentration, a relatively clean condition compared with Episode 2.

NH_4NO_3 was the largest contribution component to PM_{10} in Episode 3, accounting for 40% of the average PM_{10} mass concentration. The variations of mass-size distribution of NH_4NO_3 were similar to those of $(\text{NH}_4)_2\text{SO}_4$, following the sequence of 450–750 nm > 750–1000 nm > 250–450 nm > 0–250 nm. As shown in Fig. 5a, the OA size distributions were not as stable as those of NH_4NO_3 and $(\text{NH}_4)_2\text{SO}_4$. More of the OA mass size fraction was distributed in the 500–750 nm size range rather than 200–400 nm of the first 9 h in Episode 3, which also differed from mass-size distribution during Episodes 1 and 2. At 20:00 on December 16, the mass fraction of OA in small particles increased, but the mass concentration of OA was low. These results suggest that fresher small particles play an important role in particulate OA pollution (Qin et al., 2016). The average ammonium sulfate mass concentration was 20.9 $\mu\text{g}/\text{m}^3$ during the episode from 3:00 to 10:00 on 3 January 2017 and was 1.8 times of the episode on December 9.

The corresponding variations of OA, NH_4NO_3 , and $(\text{NH}_4)_2\text{SO}_4$ mass-size distribution for the Episode 4 were similar to those in Episode 3, specifically the highest mass-size distributions of OA, NH_4NO_3 , and $(\text{NH}_4)_2\text{SO}_4$ occurred at 550–750 nm followed by 750–1000 nm, which was correlated with $(\text{NH}_4)_2\text{SO}_4$ in Episode 3. This is probably caused by their similar sources or processes. Organic matter, NH_4NO_3 , and $(\text{NH}_4)_2\text{SO}_4$ had a consistent particle size distribution in Episode 4.

The average mass-size distributions of different aerosol constitution during the four sub-periods and clean period are shown in Fig. 6. The mass-size distribution for OA was much broader than those of NH_4NO_3 and $(\text{NH}_4)_2\text{SO}_4$ during all episodes, due to the presence of primary emissions from an ultrafine mode of OA presumably (Sun, 2010). Similar mass-size distributions for OA were also observed in Beijing, PRD (Xiao et al., 2011), Xiamen (Yan et al., 2015) and YRD (Zhang et al., 2015). However, OA mass-size distributions for different pollution episodes showed various distribution characteristics. OA represented a single peak structure in Episodes 3 and 4 as well as clean period. The peak size positions were in the range of 450–500 nm, 650–700 nm and 450–500 nm for Episode 3, Episode 4, and clean period, respectively. The peak concentration of OA showed a bimodal distribution during Episode 1 and Episode 2 with particle size peak positions were at 450–500 nm and 600–650 nm, respectively. The peak positions of NH_4NO_3 and $(\text{NH}_4)_2\text{SO}_4$ in clean period were in the range of 550–600 nm and 450–500 nm, respectively. Particle growth after typical non-pollution period events was found in our study, with the mode diameters of NH_4NO_3 and $(\text{NH}_4)_2\text{SO}_4$ showing substantial shifts toward larger sizes (up to 600 nm). There were no obvious differences between NH_4NO_3 and $(\text{NH}_4)_2\text{SO}_4$ among the haze episodes, and they had single distributions, with peaks in the 650–700 nm and ~700 nm ranges, respectively. Similar composition-specific size shifts during particle growth events have also been observed in rural PRD in summer (Xiao et al., 2009).

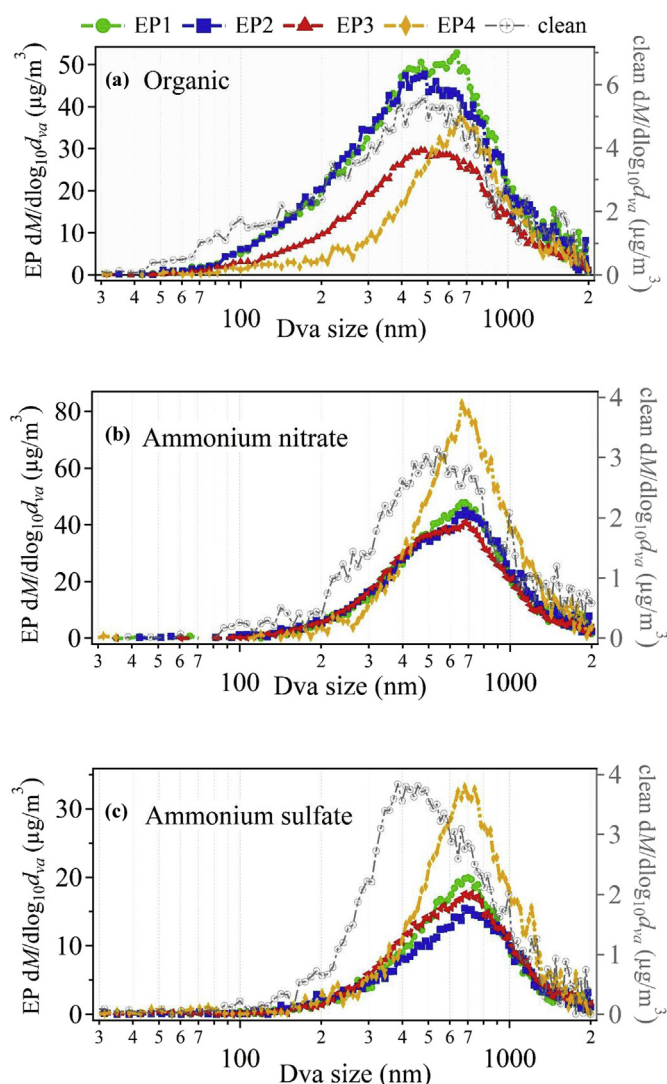


Fig. 6. The average aerosol mass concentration size distributions of individual aerosol chemical species during the four sub-periods and clean period.

3.3. Chemical apportionment of PM_1 scattering coefficient

The time series of the comparison between the scattering coefficients calculated by Mie theory and measured by PAX are shown in Fig. 7 and Fig.S2. The estimated scattering coefficient was closely correlated with the measured scattering coefficient, suggesting that the scattering coefficient estimated by Mie theory is applicable in this study. It is noteworthy that RH has an important influence on the optical properties (Chow et al., 2007). In this study, the aerosols were dried before measuring optical properties so all the discussions were excluded the effect of RH on the aerosol optical properties. The scattering coefficients are not determined by mass concentrations of PM chemical compositions alone. To provide insight into the effects that mass-size distribution of different PM_1 chemical compositions on the scattering coefficients during the pollution periods, the size distributions of the scattering coefficients were identified, as shown in Fig. 8. The average aerosol size distributions for scattering of individual aerosol chemical compounds during the four sub-periods and clean period are shown in Fig. 9.

As shown previously, mass-size distribution of OA varied in a large range before and after each pollution episode. The significant change in total scattering coefficient from $74 Mm^{-1}$ to $503 Mm^{-1}$ during pollution episodes indicated that aerosol properties change dramatically may be affected by mass-size distribution of scattering coefficient for various species. Similar patterns were observed for OA, NH_4NO_3 , and $(NH_4)_2SO_4$. The scattering coefficients increased rapidly with an increasing in mass concentration in the ranges of 450–750 nm for OA (from $\sim 100 Mm^{-1}$ to $371 Mm^{-1}$), 200–1000 nm for ammonium nitrate (from $35 Mm^{-1}$ to $149 Mm^{-1}$) and 350–1000 nm for ammonium sulfate (from $6 Mm^{-1}$ to $80 Mm^{-1}$), and they then slowly reached a plateau from 15:00 on 4 December to 11:00 on 5 December, as seen in Fig. 8.

The peak diameters for high scattering coefficient of NH_4NO_3 and $(NH_4)_2SO_4$ were in the range of 600–800 nm and 600–750 nm, respectively, so did the peak mass - size distribution during each pollution period. The peak size of OA increased from 300 to 400 nm for mass concentration and 500–650 nm for scattering coefficient. Specifically, the smaller sizes (200–300 nm) of OA had very small and stable dynamic changes in their scattering coefficient fractions when the mass concentrations of OA increased at rapid growth rates for small size and decreased in a narrow range after a few hours of pollution. Studies showed that the maximum scattering coefficients of the mono-dispersed aerosol particles usually appeared at a geometric diameter of 500–600 nm, the closer the mass particle size distribution to this range,

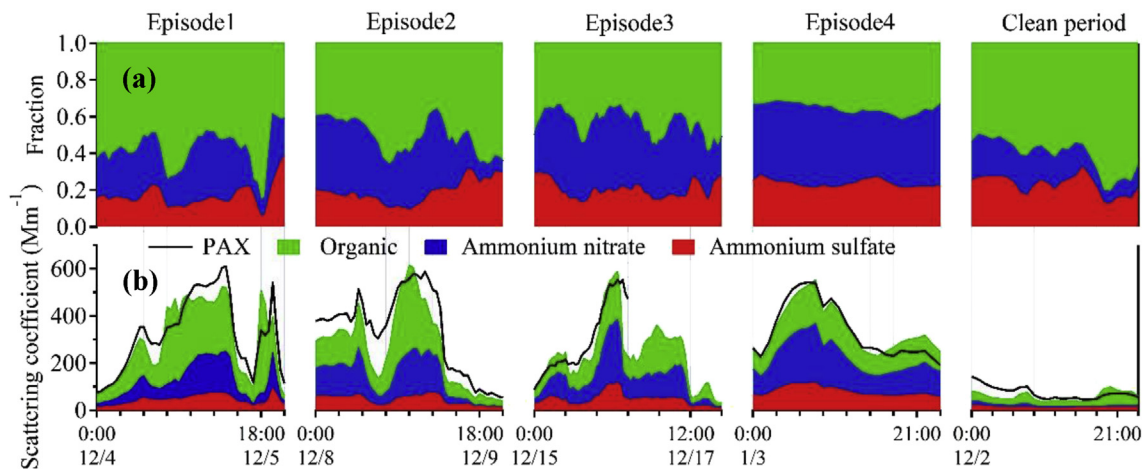


Fig. 7. Time series of (a) measured vs calculated scattering coefficient and (b) scattering fraction of organic, ammonium nitrate and ammonium sulfate during the four haze pollution Episodes and one clean episode. PAX measurement scattering coefficient are represented by black solid. The calculated scattering coefficient is the sum of scattering coefficient for organic, ammonium nitrate and ammonium sulfate.

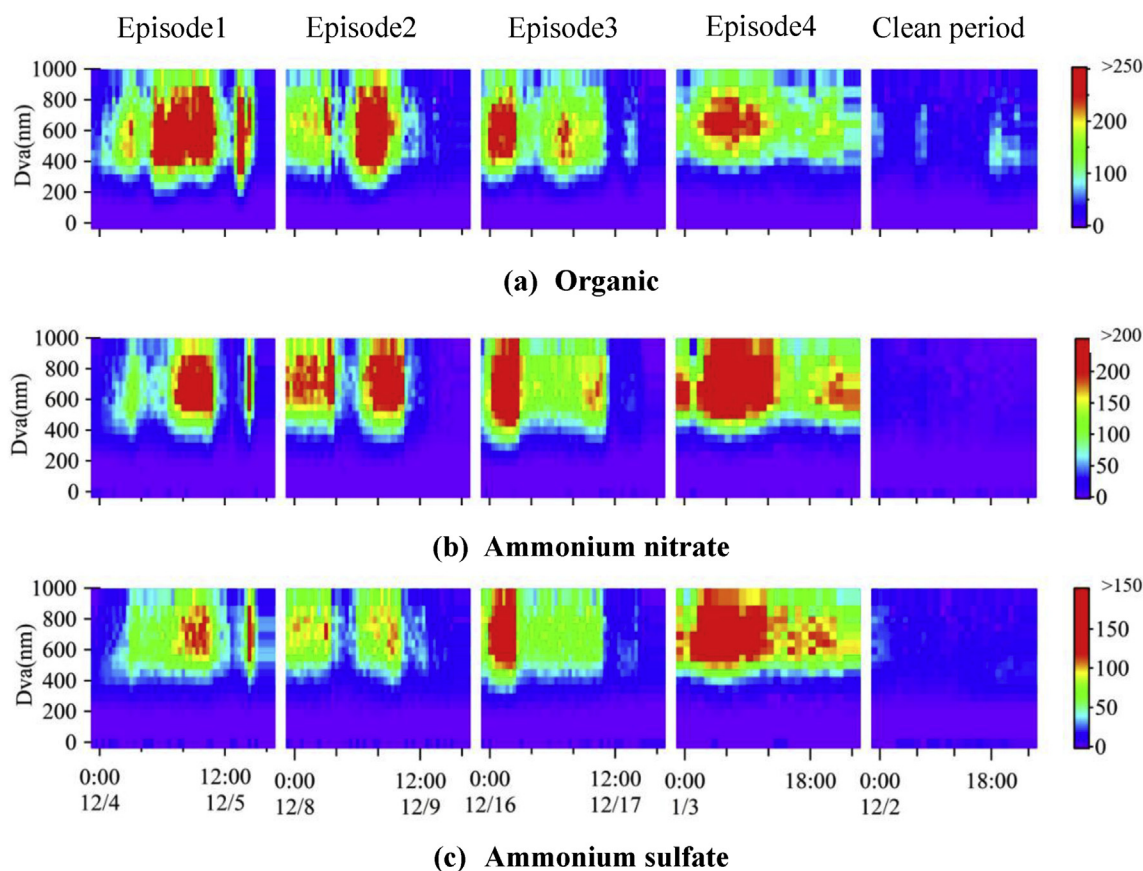


Fig. 8. Time series of size-segregated aerosol scattering coefficient of chemical compounds (Organic (a), Ammonium nitrate (b) and Ammonium sulfate (c)) during the four sub-periods and clean period. The plots are color coded by scattering coefficient (unit: Mm^{-1}) of organic, ammonium nitrate and ammonium sulfate, respectively. The values exceed the range of color scale are colored with the last color (red in the figure). (For interpretation of the references to color in this figure legend, the reader is referred to the Web version of this article.)

the higher scattering coefficients of PM species (Seinfeld and Pandis, 2012). When mass concentration of species increased, the peak sizes of OA were likely to increase toward a more effective scattering diameter range.

The average size distributions of PM_{10} scattering during clean period and pollution episodes are calculated for external mixture, as shown in Fig. 9. It was obvious that the scattering size distributions of OA were different from those of NH_4NO_3 and $(\text{NH}_4)_2\text{SO}_4$. There was a broad distribution from 100 to 500 nm in the size distribution of scattering for OA, which was consistent with mass-size distribution. Different from mass-size distribution, the scattering size distributions of OA showed a bimodal distribution in Episode 2 and clean period. OA represented a single peak structure in Episodes 1 and 3 as well as Episode 4. The peak size position was in the range of 600–700 nm, which was larger than that of mass-size distributions (400–500 nm). The scattering size distributions for NH_4NO_3 present a single peak structure during episodes and clean period, which was similar with the mass-size distribution. There was the same particle size peak at 600–700 nm in the scattering size distribution of NH_4NO_3 during Episodes 1, 3, and 4. The peak size distributions of NH_4NO_3 were in the range of larger sizes (700–800 nm) during Episode 2. The size distribution of scattering for $(\text{NH}_4)_2\text{SO}_4$ was different from that of NH_4NO_3 and OA. Specifically, the size peak positions were at larger size (700–900 nm) than those of NH_4NO_3 and OA during all of the pollution episodes. The bimodal peak positions of light scattering for $(\text{NH}_4)_2\text{SO}_4$ were at 500–600 nm and 800–900 nm in the clean period, respectively, suggesting the formation and growth of new $(\text{NH}_4)_2\text{SO}_4$ particles. In addition, the relative scattering contributions of $(\text{NH}_4)_2\text{SO}_4$ in the range of below 500 nm of clean period were greater than that of species in pollution episodes. This phenomenon was also

found in OA and NH_4NO_3 . When the particles sizes increased, the contribution of OA scattering coefficient decreased, whereas NH_4NO_3 and $(\text{NH}_4)_2\text{SO}_4$ presented an increasing trend.

In Episodes 1 and 2, OA had the largest contribution to PM_{10} scattering coefficient accounting for 54% and 53% of PM_{10} light scattering coefficients, followed by NH_4NO_3 (33% and 34%) and $(\text{NH}_4)_2\text{SO}_4$ (13% and 13%) (Fig. 7 and Fig.S2). These results mean that OA is a major factor in the degradation of visibility in Shanghai. NH_4NO_3 had the highest proportion of scattering coefficients, contributing 40% and 44% during Episode 3 and Episode 4, respectively (Fig. 7 and Fig.S2). This indicates that NH_4NO_3 contributed predominantly to the enhancement of scattering coefficient, in accordance with mass fraction that mentioned in Sect.3.1. This is consistent with the increase of nitrate resulting from the continued growth in NO_x emissions due to vehicles and industry in recent years (Wang et al., 2013). $(\text{NH}_4)_2\text{SO}_4$ was shown to be the major contributor to the scattering coefficient in previous studies in Guangzhou, Hong Kong, and Xiamen in China (Gao et al., 2015; Tao et al., 2014; Zhang et al., 2012), while our study indicated that the contribution of $(\text{NH}_4)_2\text{SO}_4$ to light scattering exceeded that of NH_4NO_3 during clean period (Fig. 7). In haze events, OA and NH_4NO_3 were the predominant contributors to scattering coefficients, with similar results reported by Yang et al. (2007). The synergistic reduction of carbonaceous species and nitrite in PM could effectively improve the visibility in Shanghai in winter.

4. Conclusions

We investigated the chemical composition, size distribution and optical properties of severe haze episodes occurred in Shanghai from

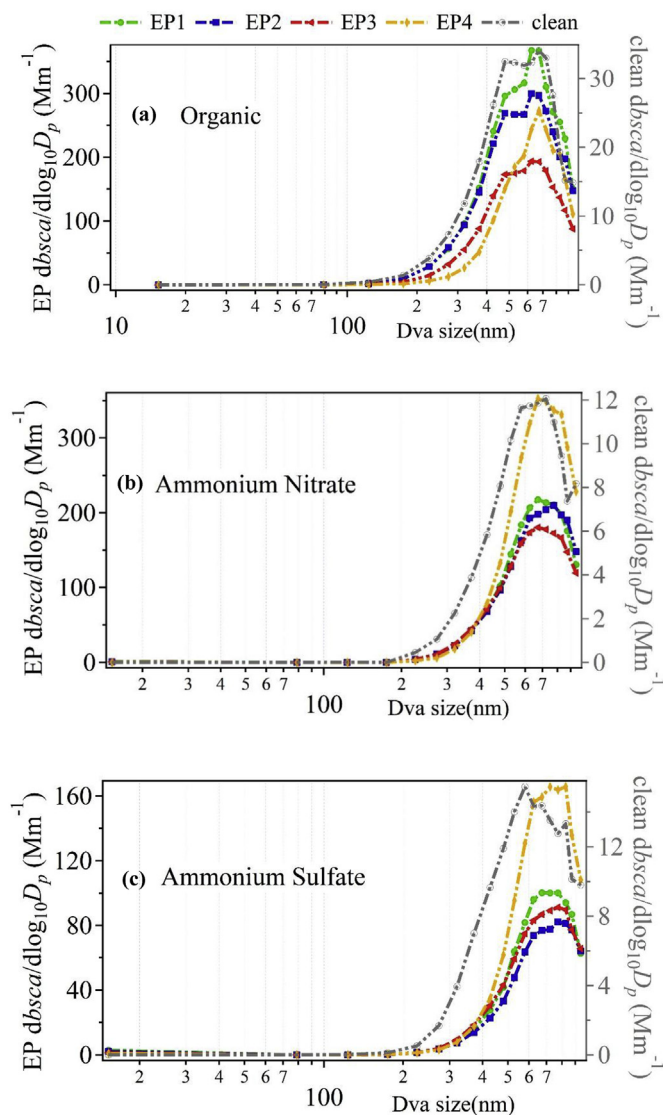


Fig. 9. The average aerosol scattering size distributions of individual aerosol chemical species during the four sub-periods and clean period.

November 28, 2016 to January 12, 2017. Four haze events were observed with the average PM_{10} scattering coefficients ranging from 486 to 542 Mm^{-1} . The mass concentrations of OA, nitrate, and sulfate increased significantly during haze episodes, and were 6–7 times greater than those of clean period. The proportions of OA and nitrate in PM_{10} increased gradually with PM_{10} increasing during Episodes 1 & 2 and Episodes 3 & 4, respectively, indicating that the enhancement of OA and nitrate primarily contributed to the increase in PM mass loading during haze pollution events. The mass-size distributions of OA for different pollution extents showed various distribution characteristics. OA exhibited a single peak structure and a bimodal distribution during haze episodes. There were no obvious differences between NH_4NO_3 and $(NH_4)_2SO_4$ among the haze episodes, which represented single distributions with peaks at 650–700 nm and ~ 700 nm, respectively.

Our results showed that the scattering size distributions of OA were different from those of NH_4NO_3 and $(NH_4)_2SO_4$. There was a broad peak from 100 to 700 nm in the scattering size distribution of OA, which was consistent with mass-size distribution. In addition, OA and NH_4NO_3 were the largest contributors to scattering coefficients of PM_{10} during the haze episodes. Our results indicated that OA ($\sim 50\%$) and NH_4NO_3 ($\sim 30\%$) primarily contributed to the scattering during haze episodes. In contrast, $(NH_4)_2SO_4$ (24%) was the second largest

contributor to scattering during clean period followed by NH_4NO_3 (20%). Taken together, these results suggest that the reduction of carbonaceous species could be just as important as controlling nitrite in Shanghai in winter. This study investigated the highly time-resolved evolution the optical properties of aerosols with changes in the mass-size distributions of the chemical components during haze pollution periods. Our future studies will be of significance in quantifying the mass-size distribution of POA and SOA, refining the scattering of OA and exploring the role of OA during haze events in greater depth.

Acknowledgments

This work is supported by the National Key Research and Development Program of China (2016YFC0208700), National Natural Science Foundation of China (21607100), National Natural Science Foundation of China (21507088) and National Natural Science Foundation of Shanghai (15ZR1434700).

Appendix A. Supplementary data

Supplementary data related to this article can be found at <https://doi.org/10.1016/j.atmosenv.2018.08.003>.

References

- Bohren, C.F., Huffman, D.R., 2008. Absorption and Scattering of Light by Small Particles. John Wiley & Sons.
- Canagaratna, M., Jimenez, J., Kroll, J., Chen, Q., Kessler, S., Massoli, P., Hildebrandt Ruiz, L., Fortner, E., Williams, L., Wilson, K., 2015. Elemental ratio measurements of organic compounds using aerosol mass spectrometry: characterization, improved calibration, and implications. *Atmos. Chem. Phys.* 15, 253–272.
- Cheung, H.C., Wang, T., Baumann, K., Guo, H., 2005. Influence of regional pollution outflow on the concentrations of fine particulate matter and visibility in the coastal area of southern China. *Atmos. Environ.* 39, 6463–6474.
- Chow, J.C., Watson, J.G., Chen, L.W., Chang, M.C., Robinson, N.F., Trimble, D., Kohl, S., 2007. The IMPROVE-A temperature protocol for thermal/optical carbon analysis: maintaining consistency with a long-term database. *J. Air Waste Manag. Assoc.* 57, 1014–1023.
- Drewnick, F., Hings, S.S., Decarlo, P., Jayne, J.T., Gonin, M., Fuhrer, K., Weimer, S., Jimenez, J.L., Demerjian, K.L., Borrmann, S., 2005. A new time-of-flight aerosol mass spectrometer (TOF-AMS)—instrument description and first field deployment. *Aerosol. Sci. Technol.* 39, 637–658.
- Gao, Y., Lai, S., Lee, S.C., Yau, P.S., Huang, Y., Cheng, Y., Wang, T., Xu, Z., Yuan, C., Zhang, Y., 2015. Optical properties of size-resolved particles at a Hong Kong urban site during winter. *Atmos. Res.* 155, 1–12.
- Garland, R.M., Yang, H., Schmid, O., Rose, D., 2008. Aerosol optical properties in a rural environment near the mega-city Guangzhou, China: implications for regional air pollution and radiative forcing. *Atmos. Chem. Phys. Discuss.* 8, 5161–5186.
- Hand, J.L., Malm, W.C., 2007. Review of aerosol mass scattering efficiencies from ground-based measurements since 1990. *Journal of Geophysical Research Atmospheres* 112, 321–341.
- Hu, W., Hu, M., Hu, W., Jimenez, J.L., Yuan, B., Chen, W., Wang, M., Wu, Y., Chen, C., Wang, Z., 2016. Chemical composition, sources, and aging process of submicron aerosols in Beijing: contrast between summer and winter. *Journal of Geophysical Research Atmospheres* 121, 1955–1977.
- Hu, W., Hu, M., Hu, W.W., Zheng, J., Chen, C., Wu, Y., Guo, S., 2017. Seasonal variations in high time-resolved chemical compositions, sources, and evolution of atmospheric submicron aerosols in the megacity Beijing. *Atmos. Chem. Phys.* 17, 9979–10000.
- Hu, W.W., Hu, M., Yuan, B., Jimenez, J.L., Tang, Q., Peng, J., Hu, W., Shao, M., Wang, M., Zeng, L., 2013. Insights on organic aerosol aging and the influence of coal combustion at a regional receptor site of central eastern China. *Atmos. Chem. Phys. Discuss.* 13, 10809–10858.
- Huang, K., Zhuang, G., Lin, Y., Li, J., Sun, Y., Zhang, W., Fu, J.S., 2010. Relation between optical and chemical properties of dust aerosol over Beijing, China. *Journal of Geophysical Research Atmospheres* 115, 346–361.
- Huang, Y., Li, L., Li, J., Wang, X., Chen, H., Chen, J., Yang, X., Gross, D.S., Wang, H., Qiao, L., 2013. A case study of the highly time-resolved evolution of aerosol chemical and optical properties in urban Shanghai, China. *Atmos. Chem. Phys.* 13, 3931–3944.
- Jimenez, J.L., Canagaratna, M.R., Donahue, N.M., Prevot, A.S., Zhang, Q., Kroll, J.H., Decarlo, P.F., Allan, J.D., Coe, H., Ng, N.L., 2009. Evolution of organic aerosols in the atmosphere. *Science* 326, 1525–1529.
- Jimenez, J.L., Jayne, J.T., Shi, Q., Kolb, C.E., Worsnop, D.R., Yourshaw, I., Seinfeld, J.H., Flagan, R.C., Zhang, X., Smith, K.A., 2003. Ambient aerosol sampling using the aerodyne aerosol mass spectrometer. *Journal of Geophysical Research Atmospheres* 108, 447–457.
- Kong, L., Yang, Y., Zhang, S., Zhao, X., Du, H., Fu, H., Zhang, S., Cheng, T., Yang, X., Chen, J., 2014. Observations of linear dependence between sulfate and nitrate in atmospheric particles. *Journal of Geophysical Research Atmospheres* 119, 341–361.

- Li, Y., Lee, B.P., Su, L., Fung, J.C.H., Chan, C.K., 2015. Seasonal characteristics of fine particulate matter (PM) based on high-resolution time-of-flight aerosol mass spectrometric (HR-ToF-AMS) measurements at the HKUST Supersite in Hong Kong. *Atmos. Chem. Phys.* 15, 37–53.
- Matthew, B.M., Middlebrook, A.M., Onasch, T.B., 2008. Collection efficiencies in an aerodyne aerosol mass spectrometer as a function of particle phase for laboratory generated aerosols. *Aerosol Sci. Technol.* 42, 884–898.
- Matzler, C., 2002. MATLAB functions for Mie Scattering and Absorption. 2002–11. Bern. Institute of Applied Physics: University of Bern.
- Ng, N., Canagaratna, M., Zhang, Q., Jimenez, J., Tian, J., Ulbrich, I., Kroll, J., Docherty, K., Chhabra, P., Bahreini, R., 2010. Organic aerosol components observed in northern hemispheric datasets from aerosol mass spectrometry. *Atmos. Chem. Phys.* 10, 4625–4641.
- Pöschl, U., 2005. Atmospheric aerosols: composition, transformation, climate and health effects. *ChemInform* 44, 7520.
- Pitchford, M., Malm, W., Schichtel, B., Kumar, N., Lowenthal, D., Hand, J., 2007. Revised algorithm for estimating light extinction from IMPROVE particle speciation data. *J. Air Waste Manag. Assoc.* 57, 1326–1336.
- Qin, Y.M., Li, Y.J., Wang, H., Lee, B.P.Y.L., Huang, D.D., Chan, C.K., 2016. Particulate matter (PM) episodes at a suburban site in Hong Kong: evolution of PM characteristics and role of photochemistry in secondary aerosol formation. *Atmos. Chem. Phys.* 16, 1–32.
- Ram, K., Sarin, M.M., Tripathi, S.N., 2012. Temporal trends in atmospheric PM_{2.5}, PM₁₀, elemental carbon, organic carbon, water-soluble organic carbon, and optical properties: impact of biomass burning emissions in the Indo-Gangetic Plain. *Environ. Sci. Technol.* 46, 686–695.
- Roger, J.C., Guinot, B., Cachier, H., Mallet, M., Dubovik, O., Yu, T., 2009. Aerosol complexity in megacities: from size-resolved chemical composition to optical properties of the Beijing atmospheric particles. *Geophys. Res. Lett.* 36, 252–260.
- Seinfeld, J.H., Pandis, S.N., 2012. *Atmospheric Chemistry and Physics: from Air Pollution to Climate Change*. John Wiley & Sons.
- Sun, J., 2010. Highly time- and size-resolved characterization of submicron aerosol particles in Beijing using an Aerodyne Aerosol Mass Spectrometer. *Atmos. Environ.* 44, 131–140.
- Sun, Y., Jiang, Q., Wang, Z., Fu, P., Li, J., Yang, T., Yin, Y., 2014. Investigation of the sources and evolution processes of severe haze pollution in Beijing in January 2013. *Journal of Geophysical Research Atmospheres* 119, 4380–4398.
- Sun, Y., Wang, Z., Fu, P., Jiang, Q., Yang, T., Li, J., Ge, X., 2013. The impact of relative humidity on aerosol composition and evolution processes during wintertime in Beijing, China. *Atmos. Environ.* 77, 927–934.
- Takegawa, N., Miyakawa, T., Kuwata, M., Kondo, Y., Zhao, Y., Han, S., Kita, K., Miyazaki, Y., Deng, Z., Xiao, R., 2009. Variability of submicron aerosol observed at a rural site in Beijing in the summer of 2006. *Journal of Geophysical Research Atmospheres* 114, 1291–1298.
- Tao, J., Zhang, L., Ho, K., Zhang, R., Lin, Z., Zhang, Z., Lin, M., Cao, J., Liu, S., Wang, G., 2014. Impact of PM 2.5 chemical compositions on aerosol light scattering in Guangzhou — the largest megacity in South China. *Atmos. Res.* 135–136, 48–58.
- Wang, Q., Sun, Y., Jiang, Q., Du, W., Sun, C., Fu, P., Wang, Z., 2015. Chemical composition of aerosol particles and light extinction apportionment before and during the heating season in Beijing, China. *Journal of Geophysical Research Atmospheres* 120, 12708–12722.
- Wang, Y., Zhang, Q.Q., He, K., Zhang, Q., Chai, L., 2013. Sulfate-nitrate-ammonium aerosols over China: response to 2000–2015 emission changes of sulfur dioxide, nitrogen oxides, and ammonia. *Atmos. Chem. Phys.* 13, 2635–2652.
- Watson, J., Chow, J., Lowenthal, D., Kl, 2008. Estimating aerosol light scattering at the Fresno Supersite. *Atmos. Environ.* 42, 1186–1196.
- Xiao, R., Takegawa, N., Kondo, Y., Miyazaki, Y., Miyakawa, T., Hu, M., Shao, M., Zeng, L.M., Hofzumahaus, A., Holland, F., 2009. Formation of submicron sulfate and organic aerosols in the outflow from the urban region of the Pearl River Delta in China. *Atmos. Environ.* 43, 3754–3763.
- Xiao, R., Takegawa, N., Zheng, M., Kondo, Y., Miyazaki, Y., Miyakawa, T., Hu, M., Shao, M., Zeng, L., Gong, Y., 2011. Characterization and source apportionment of submicron aerosol with aerosol mass spectrometer during the PRIDE-PRD 2006 campaign. *Atmos. Chem. Phys.* 11, 6911–6929.
- Xu, L., Penner, J.E., 2012. Global simulations of nitrate and ammonium aerosols and their radiative effects. *Atmos. Chem. Phys.* 12, 9479–9504.
- Yan, J., Chen, L., Lin, Q., Li, Z., Chen, H., Zhao, S., 2015. Chemical characteristics of submicron aerosol particles during a long-lasting haze episode in Xiamen, China. *Atmos. Environ.* 113, 118–126.
- Yang, L., Zhou, X., Wang, Z., Zhou, Y., Cheng, S., Xu, P., Gao, X., Nie, W., Wang, X., Wang, W., 2012. Airborne fine particulate pollution in Jinan, China: concentrations, chemical compositions and influence on visibility impairment. *Atmos. Environ.* 55, 506–514.
- Yang, L.X., Wang, D.C., Cheng, S.H., Wang, Z., Zhou, Y., Zhou, X.H., Wang, W.X., 2007. Influence of meteorological conditions and particulate matter on visual range impairment in Jinan, China. *Sci. Total Environ.* 383, 164.
- Yu, X., Zhu, B., Yin, Y., Yang, J., Li, Y., Bu, X., 2011. A comparative analysis of aerosol properties in dust and haze-fog days in a Chinese urban region. *Atmos. Res.* 99, 241–247.
- Zhang, F., Xu, L., Chen, J., Yu, Y., Niu, Z., Yin, L., 2012. Chemical compositions and extinction coefficients of PM 2.5 in peri-urban of Xiamen, China, during June 2009–May 2010. *Atmos. Res.* 106, 150–158.
- Zhang, Q., Canagaratna, M.R., Jayne, J.T., Worsnop, D.R., Jimenez, J.L., 2005. Time- and size-resolved chemical composition of submicron particles in Pittsburgh: implications for aerosol sources and processes. *J. Geophys. Res.: Atmosphere* 110.
- Zhang, X., Zhang, Y., Sun, J., Yu, Y., Canonaco, F., Prévôt, A.S., Li, G., 2017. Chemical characterization of submicron aerosol particles during wintertime in a northwest city of China using an Aerodyne aerosol mass spectrometry. *Environ. Pollut.* 222, 567–582.
- Zhang, Y.W., Zhang, X.Y., Zhang, Y.M., Shen, X.J., Sun, J.Y., Ma, Q.L., Yu, X.M., Zhu, J.L., Zhang, L., Che, H.C., 2015. Significant concentration changes of chemical components of PM1 in the Yangtze River Delta area of China and the implications for the formation mechanism of heavy haze-fog pollution. *Sci. Total Environ.* 538, 7–15.